Review Article

Hongcai Li#, Shuanqiang Yang#, David Hui, and Ruoyu Hong*

Progress in magnetic Fe_3O_4 nanomaterials in magnetic resonance imaging

https://doi.org/10.1515/ntrev-2020-0095
received August 4, 2020; accepted September 30, 2020

Abstract: At present, high-sensitivity, high-penetration-depth, and accurate tissue resolution clinical imaging effect are required, while computer transverse scanning, microwave imaging, and fluorescence imaging (FL) cannot meet the requirements of clinical imaging, but the magnetic resonance imaging (MRI) can meet the requirements of clinical dissecting details. The effect of MRI imaging is closely related to the contrast agent (CA). As an important type of CA, Fe_3O_4 and its analogues have been widely concerned because of their low toxicity and relatively low price. In this review, we summarize the development and improvement of CAs based on Fe_3O_4 and its analogues from T_2 imaging mode and development limitation in the initial single modulus imaging mode, to T_1 imaging mode overcoming the limitations of T_2 imaging and the limitations of its own in application, to the later development of dual modulus imaging form, and to the current multi-modulus imaging form. Simultaneously, we demonstrate the research progress, preparation methods, and future trends based on Fe_3O_4 and its analogues CAs for MRI, the current application status is preliminarily summarized, and the future development trend is prospected.

Keywords: RI, Fe_3O_4 nanoparticles, preparation, imaging mode, imaging effect

1 Introduction

Nowadays, the early diagnosis of various difficulty and miscellaneous diseases, such as cancer and septicemia, has always been a difficult problem in medicine. Therefore, the key to solve this problem is the effective auxiliary diagnosis method [1]. Magnetic resonance imaging (MRI) is one of the most powerful medical diagnosis methods because of the images provided by MRI with excellent anatomical details based on soft tissue contrast and functional information in noninvasive, real-time monitoring manner [2]. Compared with computer transverse (CT), sonography, nuclear scintigraphy, and X-ray imaging, MRI causes no radiation damage and provides high soft tissue resolution, and hence can be applied to diagnose a variety of diseases [3]. However, conventional MRI contrast agent (CA) is expensive, low in spatial resolution, which fails to detect early tiny tumors, and cannot distinguish between benign and malignant tumors because of current CAs having only a single imaging mode [4]. The results of the MRI are determined by not only the precision instrument and different imaging methods, but also the CA, which can significantly improve the contrast of the biological targets around the tissue [5]. Therefore, the development of new CAs can effectively improve the imaging effect.

From the application point of view, CAs can be divided into two categories, one is the longitudinal relaxation T_1 signal CA (r_1) that produces the bright field as a positive CA, and the other is the transverse relaxation T_2 signal CA (r_2) that produces the dark field as a negative CA [6]. The T_1 signal is generated by the interaction between the outermost electron cloud of the magnetic element and the protons in the water to produce a bright signal, whereas the T_2 signal is a darker signal owing to the magnetic unevenness caused by the strong magnetic moment [7]. In terms of production mode, relaxation direction, and field of view, the two categories of CAs are totally different; however, the division method is generally accepted, especially for products with better circulation in the market [8].

# These authors contributed equally to this review.

* **Corresponding author: Ruoyu Hong,** College of Chemical Engineering, Fuzhou University, Fuzhou, Fujian 350108, China, e-mail: rhong@fzu.edu.cn
Hongcai Li: College of Chemical Engineering, Fuzhou University, Fuzhou, Fujian 350108, China
Shuanqiang Yang: Institute of Industrial Technology, Fujian Jiangxia University, Fuzhou, Fujian 350108, China
David Hui: Department of Mechanical Engineering, University of New Orleans, New Orleans, LA 70148, United States of America

Gadolinium has been a popular product in the market on account of its T_1 signal as an MRI CA [9]; however, the recent FDA warning about the increased risk of nephrogenic systemic fibrosis and nephrogenic fibrosing dermopathy in patients who suffer from renal failure and are subjected to enhanced contrast MRI exams has given rise to concern [10]. Therefore, the development of new CAs to meet clinical needs has attracted much attention. Super-paramagnetic iron oxide magnetic nanoparticles (SPIONs) and uniform ferrite nanoparticles such as Fe_3O_4 and Fe_2O_3 are widely applied in magnetic nanoparticle (MNP)-based CAs because of their non-toxicity and biodegradability [11]. Different forms of ferrite MNPs have been well reported in the literature for decades because of their countless biomedical applications, including MRI [12], targeted drug delivery [13], photothermal [14], and magnetic fluid hyperthermia cancer therapy [15]. These applications are based on excellent features, such as super para-magnetism, possibility of tuning of particle size (for desired electrical, optical, and magnetic properties) [16], mono-dispersity, stability, biocompatibility, large surface areas that can be easily functionalized [17], improved magnetic sensitivity, and range of different synthesis methods [18]. In this review, the synthesis methods, outsourcing materials, and doping metal methods of ferroferric oxide nanoparticles are described. From the perspective of imaging methods, combined with the description of biological applications, a detailed discussion of the problem, current solutions, and prospects for the application of ferroferric oxide for MRI imaging were provided.

2 Single modulus imaging

Because the FDA announced the toxicity of gadolinium to the kidneys, MNPs have attracted more attention [19]. The outermost layer of iron has five electrons with strong magnetism, so can generate vivid MRI signals, allowing rapid development of MNPs.

2.1 T_2 sign imaging of Fe_3O_4 nanomaterials

Ferrites are crystalline iron oxides whose magnetic properties were recognized for their commercial importance as early as 1933 [20]. Ferrites have the general formula $Fe_2^{3+}O_3{\cdot}M^{2+}O$, where M is a divalent metal ion such as manganese, nickel, iron, cobalt, or magnesium. Magnetite is a naturally occurring ferrite in which the metal ion (M) is a ferrous iron (Fe^{2+}). More importantly, the outermost layer of iron atom contains five electrons similar to gadolinium, which can change the relaxation time of protons and engender greater r_1 and r_2 relaxation effects, thus showing certain potential in MRI applications [21]. So far, there are three kinds of iron CAs using the T_2 sign imaging on the market, Feridex (r_2 = 120 $mM^{-1}\,s^{-1}$), Resovist (r_2 = 186 $mM^{-1}\,s^{-1}$), and Combidex (r_2 = 65 $mM^{-1}\,s^{-1}$), respectively [22]. The following is in introduction to the current T_2 CA study.

The stability of CAs is one of the key problems affecting the application of CA [23]. Researchers have tried various ways in which to improve the stability without changing the magnetic imaging performance. Among them, the copolymerization of an organic polymer is a relatively direct and an effective method [24]. There are two preparation methods available: (i) one is to first synthesize nanoparticles and then to modify the coating with an organic polymer, and (ii) one-pot method by thermal precipitation copolymerization method [25] (Figure 1).

Certainly, there are other ways, for example, Kluenker et al. [26] presented a solution phase seed mediated synthesis of iron oxide superparticles colloidal with flower- and hedgehog-like morphologies starting at dispersible spherical maghemite and nanoplate hematite (HEX) templates to overcome the drawbacks of particle assemblies for functional nanodevices such as low mechanical stability, lack of interfacial electronic communication, and poor processability [27]. Changes in solvent, type of iron salts, and temperatures have been used to synthesize different types of nanomaterials (Figure 2; the NPs are mostly spherical and faceted, and an average particle size is 18–20 nm). As for the higher effective radius and anisotropy and inhomogeneity of the particle-generated magnetic field, both longitudinal and transversal relaxation sign effects show obvious enhancement (r_1 and r_2 values are 0.093 and 1.774 $mM^{-1}\,s^{-1}$ for HEX SPs). The r_2 relaxivity could be increased by a factor 2.5–64.36 $mM^{-1}\,s^{-1}$ showing the potential for application

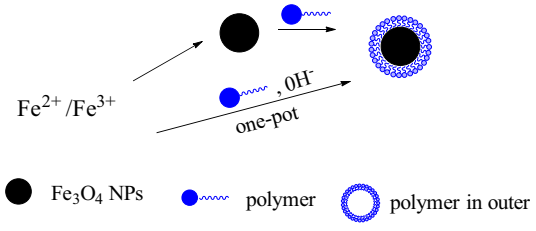

Figure 1: Preparation methods of iron CAs.

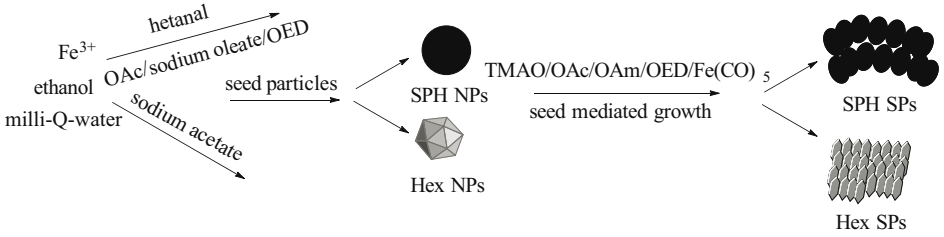

Figure 2: Flow diagram of solvent planting process [26].

as a T_2 CA. Generally, the viability of the cells decreases with increasing Fe concentration and reaches a minimum of 70–80% at 100 μg/mL NPs, which exhibits less virulence. Certainly, this preparation method also provides a new way for industrial production.

Early organic polymer coating with dextran, polyethylene glycol (PEG) [28], polyvinyl alcohol, and chitosan as an outer cladding has been reported [29]. These polymers can effectively improve the water solubility and stability of nanomaterials, but the size of nanoparticles is also significantly increased, relevant studies were shown below.

Hong et al. [30] coated SPIONs with dextran to stabilize monocrystalline structures to form a stable magnetic fluid, so the stability and biological properties of dextran-coated SPIONs were significantly improved, but its application was limited by the larger particle size. Mailander et al. [31] modified Resovist (generic name: ferucarbotran) with carboxydextran in Feridex (ferumoxides) and original dextran. Many studies have shown that the PEG coating of iron oxide nanoparticles (IONPs) improves their stability (with a mean diameter (S_d) of 10 nm) [32]. Although pure PEG can improve the stability of IONPs, it will soon be removed by the *RES* system. Therefore, PEG can act as remedy for such defects. For example, Xie et al. [33] stabilized oleic acid/oleylamine coated NPs by PEG-dopamine, which demonstrated a remarkable abatement in nonspecific uptake by macrophage cells. Amstad et al. [34] proved the better stability of PEG compounds bound to iron oxide NPs coated by nitrocatechols compared to that with catechols. In recent years, research on other types of polyorganisms has gradually increased, such as amino acids and phosphate polymers [35].

At present, the clinical contrast medium should not only be stable enough and non-cytotoxic, but also meet the requirements of low dose, a certain degree of targeting, and so on [36]. Therefore, it is imperative to improve its magnetic properties while achieving targeted properties. Monoclonal antibodies (MAbs) could distinguish malignant tumors from normal tissue and could be used for selective targeting [37]. Kubovcikova et al. [38] coated ferric material with poly-lysine (MFPLL, S_d = 85 nm, and a hydrodynamic diameter (H_d) of 119.2 nm) to improve the stability in aqueous solution, and then conjugated a selected specific antibody VII/20 (Ab-MFPLL, with a S_d of 128 nm, and a H_d of 170.1 nm), which was capable of internalization and targeting to recognize the overexpression of carbonic anhydrase IX (CAIX) in tumors. Stability studies show that Ab-MFPLL and MFPLL are stable in acidic conditions up to pH = 6 and alkaline medium up to pH = 8, respectively. Simultaneously, MFPLL showed a notable enlargement in H_d after 44 h at room temperature, and the Ab-MFPLL showed no changes throughout the 74 h experiment, proving their excellent stability. The relaxivity values r_2 and r_1 of MFPLL were 487.94 and 1.81 $mM^{-1} s^{-1}$, respectively, and the ratio r_2/r_1 equaled to 270, which proved the potential as T_2 CA [39]. Furthermore, Ab-MFPLL samples preserve the property of magnetic hyperthermia differing from other USPIOs [40]. The specific absorption rate values of MFPLL were 14–15 W g^{-1} at a frequency of 190 kHz and field strength of *c*. 8 kA m^{-1}, which evinces the potential for the application of magnetic hyperthermia. Yin et al. [41] used targeted peptide WSGPGVWGASVK (peptide-WSG) conjugated Fe_3O_4 NPs coated with dextran (SPIONs@Dex-WSG), to meet practical requirements. Preparation of SPIONs@Dex-WSG relies on use of sodium citrate as an intermediate material to connect WSG and SPIONs@Dex. The average size of SPIONPs@Dex-WSG (60.66 nm) decreased compared with SPIONPs@Dex (165.20 nm) because SPIONs@Dex-WSG can significantly improve the agglomeration of nanoparticles, avoiding their elimination by *RES*, and prolonging blood circulation time. Cytotoxicity experiments showed that SPIONs@Dex-WSG was only slightly toxic to SKOV-3 uterine cancer

cells and non-toxic to normal cells. Simultaneously, Prussian blue staining indicates that only SKOV-3 uterine cancer cells appeared blue while normal cells were not stained, which indicated that SKOV-3 uterine cancer cells had good targeting and a weak inhibition rate. Its plasma half-life was as high as 10.6 h, which also provided support for its enrichment in tumors. The VSM and T_2 for SPIONs@Dex-WSG were 44.65 emu g^{-1} and 229.70 mM^{-1} s^{-1}, respectively.

The outer layer is either dextran or amino acid, and its bonding mode is nothing more than a carbon–oxygen bond or a carbon–nitrogen bond [42]. When the external environment changes, it is easy to break the structure of nanoparticles and release SPIONs, resulting in reduced stability. Demin et al. [43] formed a stable P–O–Fe bond by the coordination of phosphate on PMIDA (1:1, mol/mol) with the iron of MNPs (PMIDA@Fe_3O_4 NPs) and obtained an optimum condition for the modification of MNPs at reaction at 40°C for 3.5 h; at the same time, PMIDA exhibits selectivity recognizing for HER-2 receptors in MCF-7 tumor cells [44]. PMIDA@Fe_3O_4 NPs had good colloidal stability (concentration = 0.1–2.8 mg/mL, pH = 2–11) and high magnetic properties (with values r_2 and r_1 were 341 and 102 mM^{-1} s^{-1}, respectively). PMIDA@Fe_3O_4 NPs as a T_2 contrast agent was demonstrated in the first time for liver studies *in vivo* (dose of 0.6 mg kg^{-1}).

Although the organic outer polymer cladding layer can improve the stability of IOSNPs, it is the low magnetic sensitivity that still limits their further application [45]. The ability of MNPs was affected with shape and composition engineering. Yin and colleagues [46] doped dysprosium (the magnetic moment of Dy (10.6 μ_B) was 3.5 times larger than Fe) into Fe_3O_4 nanoparticles and coated it with polyethylene alcohol on its outermost layer to improve the sensitivity of IOSNPs. The r_2 value was 123.2 s^{-1} mM^{-1}, which was nearly double than the pure IOSNPs (67.8 s^{-1} mM^{-1}) and substantially surpassing that of Feridex and Resivist [47]. More importantly, low dose doping did not cause a toxic reaction, but *in vivo* imaging was yet to be reported. Yin and colleagues only considered the composition of the nanoparticles, without considering the influence of the shape of them. Gao et al. [48] not only considered the configuration of nanoparticles, but also studied the effect of the different metal doping ratio on the properties of nanoparticles. They manufactured zinc ferrite octapods ($Zn_xFe_{3-x}O_4$) with different Zn ratios, and studied an effect of the different ratios of Zn in $Zn_xFe_{3-x}O_4$, indicating that $Zn_xFe_{3-x}O_4$ (x = 0.44) with octahedral structure owns a notable M_s of 89.0 emu/g and r_2 value of 989.1 mM^{-1} s^{-1}. The specific production steps are as follows: $FeCl_3$ was reacted with sodium oleate in a mixed solution of ethanol and distilled water (v/v = 1:1) for 4 h, filtered after cooling, and the red oil layer was collected and concentrated, which contains iron oleate. Zinc oleate was used in the same way (temperature increased to 100°C for 0.5 h after dissolving the metal salt, and then impurities removed). Under the protection of N_2, $Zn_xFe_{3-x}O_4$ octapods were realized by calcination at 350°C for 2 h, where x represents the ratio of iron oleate to zinc oleate. The sensitive detection can be even 0.7 mM lower for orthotopic and metastatic hepatic tumors (1/10 for the clinical dose), which demonstrated the potential as a T_2 CA [49].

Similarly, nanomaterials mixed with other metals can improve contrast performance and have favored attentions interest recently [50]. Luminomagnetic nanoparticles that possessed core/shell structures (and Fe_3O_4 NPs coated with luminescent material) show some advantages [51]. Although optical imaging and magnetic imaging can be achieved because of the existence of rare earth up-conversion fluorescent nanoparticles, the imaging effect is not ideal, especially magnetic imaging [52].

Karthi et al. [53] doped Nd^{3+} to fluorapatite (FAP) and coated Fe_3O_4 nanoparticles by a hydrothermal method. The specific preparation method is as follows: adding Nd^{3+} droplets to Fe_3O_4 nanoparticles coated with FAP, while maintaining an alkaline environment and calcining at 600°C for 1 h, the final product was obtained (FFN, in rod shaped with average length 40 nm). It exhibited a superparamagnetic property (M_s of FFN is 1.3 emu/g at 1.6 mT) and showed excellent optical properties (emission at 1,060 nm). Cytotoxicity results indicated that when the concentration reached 500 μg/mL, the *L929* cell survival rate remained up to 84%, showing good biocompatibility, but the real imaging effect was not discussed.

Whether using doped metal or researching the outer layer, it is necessary to improve the performance of CAs and advance their clinical application. As an iron agent for the T_2 signal, such research is extensive, and its biological applications likewise [54]. To further improve the biological performance of CAs, Chandra and colleagues [55] modified amino acid (aa) into ferrite to prepare the magnetic fluid (Fe^{3+}:Fe^{2+}:aa = 1:2:3, particle size about 15 nm) for the first time. It can be used to image stem cells because of the coating of amino acid, so the biological toxicity of magnetic fluid is trivial. The theoretical basis is that amino acids can be used in vaccine research and development, and ideal biocompatibility makes it stable in the body; what is more interesting is that MRI is applied to MSCs imaging for the first time [56]. The imaging effect showed that its T_2 imaging effect was

better than that of pure ferrite and commercial magnetic fluid, showing the amino acid-modified magnetic fluid's relative advantage for T_2 MRI in MSCs.

Similarly, Li and colleagues [57] have also used ferrite for its magnetic properties and MRI performance to prepare a special purpose ferrite coated with CPG (forming a lecithin-like structure) and anti-*CD205*. Targeted *CD205* and bionic CPG were used to transport ferrite to lymph nodes to achieve real-time monitoring of lymph nodes. The results showed that T_2 imaging of lymph nodes was superior to its performance in other organs and proves that ferrite has been effectively transported to the lymph nodes.

VEGF-A is a cytokine overexpressed in benign or metastatic cancer cells, such as breast, ovarian, cervical, lymphoma, and colon, as well as in other cell lines such as epithelial cells [58]. Ma et al. [59] coated oleic acid–Fe_3O_4 and triphenylamine-divinylanthracene-dicyano (TAC) with poly(L-lactic-coglycolic acid) by O/W method. Simultaneous modified anti-VEGF antibodies were used to form anti-VEGF/OAFe_3O_4/triphenylamine-divinylanthracene-dicyano@poly(L-lactic-*co*-glycolic acid) NPs. This system was capable of recognizing overexpressed VEGF-A at as low as 68 pg/mL in different cell lines. The r_2 reached 86.2 mM^{-1} s^{-1}, and the magnetic resonance signal appeared within 30 min by intravenous injection and reached the peak at 60 min in tumors, which proved its good selectivity. At the same time, the optical properties of the TAC can be used to achieve photothermal therapy while imaging, to achieve the integration of diagnosis and treatment.

The instability of CAs in colloid and the difficulty in drug release limit its clinical application *in vivo* [60]. To solve the problems of unstable micelles *in vivo* and difficulty in drug release, Yang et al. [61] used organic thiol-based silicon as the outermost layer of micelles. Specific steps are as follows: (i) based on the self-assembly characteristics of polycaprolactone-*block*-poly(glutamic acid) (PCL-*b*-PGA) in aqueous solution, Fe_3O_4 nanoparticles and doxorubicin (Dox) were initially coated as the core; (ii) a thiol-containing silicone layer was formed on the outer layer with the help of 3-mercaptopropyltrimethoxysilane to form biodegradable nanoparticles (Fe_3O_4/Dox NPs); and (iii) PEG was modified on the outer layer of Fe_3O_4/Dox NPs (FDPOMs, with S_d of 120 nm). The M_s of FDPOMs was 7.4 emu g^{-1}, which was lower than the pure Fe_3O_4 NPs (33.2 emu g^{-1}) because of the outermost organic layer and organosilica components surrounding the Fe_3O_4 nanoparticles [62]. The r_2 value of FDPOMs was 192.06 mM^{-1} s^{-1} *in vivo*; interestingly, the tumor region showed the strongest T_2 sign after injecting FDPOMs for 4 h, which demonstrates that the FDPOMs own potential as T_2 CA. The outermost layer contains sulfhydryl, so it can be degraded by glutathione, thus releasing drugs in the tumors, making the tumor inhibitory 7.9 times higher than that of Dox alone [63], however, due to the presence of Dox, the biological toxicity is high, when the adriamycin content exceeded 25 μg/mL, the cell survival rate was less than 50%.

2.2 T_1 sign imaging of Fe_3O_4 nanomaterials

Defects of T_2 signal imaging are gradually exposed, the dark view produced by transverse relaxation easily causes confusion in diagnosis, and strong magnetic distance causes "bioboming effect" generating an interference magnetic area [64]. T_1 signal imaging is a bright field of vision produced by longitudinal relaxation, which can overcome the defects of T_2 signal application [65].

When reducing the effective particle size of the nanoparticles, the value of surface area/volume ratio is effectively increased, causing accumulation; in addition, the outermost layer of iron atoms contains five lone pairs of electrons, which can generate a high T_1 [66]. Based on this idea, Wei et al. [67] studied zwitterion-coated-ultra-SPIONs (ZES-SPIONs, the S_d was 4 nm). Although ZES-SPIONs demonstrated excellent T_1 imaging potential and biocompatibility, the preparation process is complicated and polluting, especially the sophisticated phase transition process, and therefore its practical application is limited.

Hao et al. [68] applied zwitterion to improve the preparation method. The improved preparation has two innovations: (1) preparing amphiphilic dopamine sulfonate (ZDS) as the outer layer to improve the application of dopamine; and (2) using diethylene glycol as solution and adopting two-step method to obtain Fe_3O_4 NPs coated with ZDS (ZUIONs). The size of ZUIONs was only 3.3 nm and the H_d was 7.0 nm; more importantly, it showed perfect stability, and above all, the program only needed one pot. The nanoparticles improve the T_1 signal (r_2 = 2.4 mM^{-1} s^{-1} and an r_2/r_1 = 2.2 at 1.0 T); meanwhile, it is exciting that it has showed enough cycle time without any immune response and metabolism. To sum up, it shows great clinical application value, but only as a T_1 CA.

Li et al. [69] also developed biodegradable Fe_3O_4-coated catecholate amphiphilic block to improve imaging effect and stability, but the complicated preparation is limited for its application as it requires multi-step reactions to guarantee the amphipathy. Miao et al. [70]

applied α-amino acid *N*-thiocarboxyanhydrides (NTAs) with polysarcosine (PSar) to synthesize poly-3,4-dihydroxy-L-phenylalanine-*b*-polysarcosine (PDOPA-*b*-PSar) via controlled ring-opening polymerizations, and then PDOPA-*b*-PSar coated Fe_3O_4 NPs to get micellar nanoparticles of Fe^{3+}@PDOPA-*b*-PSar, which simplifies the process of production, including phenol hydroxyl protection and deprotection and so on, so as to facilitate future industrial production. Fe^{3+}@PDOPA-*b*-PSar not only shows the higher ability of T_1 MRI (3.0 T, 20°C) but also exhibits a longer circulation time (2.5 h) compared to commercial Gd^{3+} and DTPA-Gd^{3+}. Simultaneously, their biocompatibility is excellent when evaluated in *NIH 3T3* cells, but the release and metabolism of Fe^{3+} *in vivo* and absence of T_2 signal MRI were not considered by the authors.

The composition of the outer cladding and the length of the chain layer will affect the magnetic properties and biological properties of the final nanoparticle [71]. Fortin et al. [72] used poly[oligo(ethylene oxide) monomethyl ether methacrylate] (POEOMA) covalently connected with either poly(methacrylic acid) (PMAA) as an anchoring block to increase blood retention time [73]; at the same time, brushed-PEG chains were applied to ensure the branching state (straight chains become brushed chains, *P2*). The preparation process was designed to replace chain PEG with brushed-PEG: because of the presence of a large number of –COOH radicals, the intermolecular force was greater and the particle size is smaller, but the zeta charge was reduced to –1. There was no obvious precipitation to prove the stability of –COOH radicals in 72 h of blood compatibility experiment. *In vitro* T_1 imaging for *P2* showed that the values of r_1, r_2, and r_2/r_1 were 5.3 $mM^{-1}\,s^{-1}$, 20.7 $mM^{-1}\,s^{-1}$, and 3.8, respectively, which were significantly lower than chain-like outsourcing, but higher than commercially available Supravist SHU-555C [74]. *In vivo* angiography showed that there was a strong signal at 2 h (blood half-lives 2–5 h), which was mainly related to the presence of more –COOH in the outer layer.

The magnetic properties are independent of the type of external coating and are widely studied. At the same time, the phenomenon of ferroptosis therapy (FT) appeared in people's vision, conferring a huge advantage in the diagnosis and treatment, and thus received much attention [75].

Since Dixon et al. first proposed FT in 2012 [76], it has been found that the FT efficacy was low because the high concentration of iron in the treatment process was demanded (75 mg iron/kg mice, the principle is shown in Figure 3) and FT therapy has not been used in the treatment of brain tumors, which is that metallic

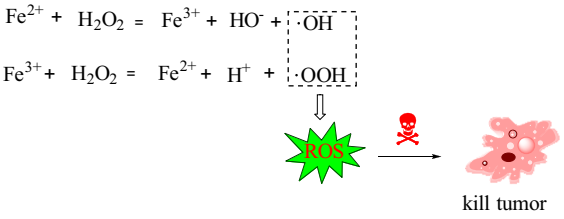

Figure 3: The principle of FT for killing cancer cells.

nanoparticles are toxic to the central nervous system and difficult to penetrate the blood–brain barrier (BBB) [77].

To effectively cross the BBB, Shen et al. [78] prepared Fe_3O_4/Gd_2O_3 NPs loaded cisplatin (CDDP) and modified lactoferrin (LF) and RGD dimer (RGD2) (FeGd-HN@Pt@LF/RGD2) to improve FT efficacy by synchro raising the topo-reactants' concentrations (Fe^{2+}, Fe^{3+}, and H_2O_2) in tumor cells, and to cross the BBB and reach the tumor cells by LF receptor, RGD2 receptor, and their small size (6.6 nm). The FT mechanism is as follows: when entering the brain, Fe^{2+}, Fe^{3+}, and CDDP can be released from the nanoparticles after endocytosis, NADPH oxidases can be activated by CDDP to produce H_2O_2, and all reactants work together to generate reactive oxygen species, causing brain cancer death. These nanoparticles are a potential T_1 CA as for the high r_1 value (56.57 $mM^{-1}\,s^{-1}$) and low r_2/r_1 (1.25) at 1.5 T, which can be ascribed to the special morphological results and ease of access to water. Furthermore, the cure rate for the tumor mice was nearly 100% after 18 days treatment, which exhibits an excellent FT effect.

The FT effect has a good therapeutic effect and a certain degree of targeting, and certain clinical application potential. Of course, there are other applications, such as in liposomes and vesicles. Madhuri et al. [79] cleverly coated the inner layer with polymersome and Gd nanoparticles, and simultaneously targeted the surface folate and the chemotherapeutic drug methotrexate on the surface modification to reform the magnetopolymersome (MPS). When achieving the target, the chemotherapeutic drug was released, so as to achieve the purpose of simultaneous effect of chemotherapy. Gold nanoparticles for targeted dual-mode therapy and imaging have been used. MPS has high biocompatibility because of its identical structural analogues with the cell membrane and also achieves high drug loading and targeting as well as development imaging. The r_1 and r_2 of prepared AuNFs@MPS were 60.57 and 200.0 $mM^{-1}\,s^{-1}$, respectively ($r_2/r_1 = 3.3$), which proved that AuNFs@MPS was potential as T_1 MRI CA [80]. Although it can realize multi-mode treatment and diagnosis, the production

process is cumbersome and is not suitable for further development.

3 Dual modulus imaging

The T_1 CAs can produce bright vision, but it often obscures with biomasses calcification and fat tissues, for example. However, the dark field of view produced by T_2 imaging is an indelible defect in accurate diagnosis [81], so the development of bimodal imaging can complement each other and improve the accuracy of diagnosis. In this review, the development process and trend of dual-mode imaging are described, as shown in Figure 4, and the details are shown below.

3.1 Application of Fe_3O_4 in bimodal imaging

Reducing the particle size of the nanoparticles not only produces a higher T_1 signal, but also controls the particle size to generate a simultaneous T_2 signal for dual-modulus imaging. The preparation method is mostly based on thermal decomposition [82], as shown below.

Since 2005, Chen et al. [83] used dodecanethiol-polymethacrylic acid (DDT-PMAA) to prepare 1–4 nm single-layer gold nanoparticles, providing theoretical support for preparation of ultra-small-MNPs. Cooper et al. [84] used this principle to first synthesize the ligand of trithiol-terminated poly(methacrylic acid) (PMAA-PTTM), which was then used to synthesize ultra-small magnetic Fe_3O_4 nanoparticles, but it did not apply it for MRI. Who is really applied those nanoparticles to MRI is Li et al. [85], who prepared monodispersed hydrophilic ultra-small Fe_3O_4 NPs (UMIONs, D = 3.3 ± 0.5 nm) for detailed MRI imaging

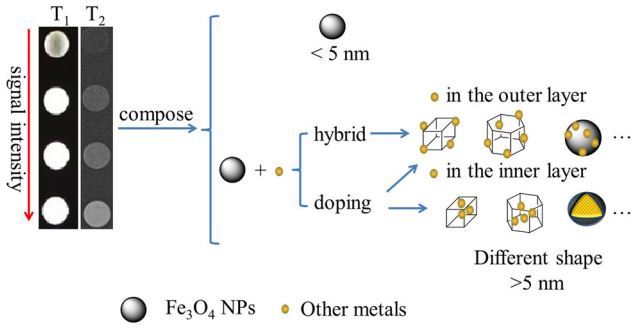

Figure 4: Composition and current situation of dual modulus imaging.

performance studies. The results showed that their longitudinal relaxivity value at 4.7 T (r_1 = 8.3 $mM^{-1}\,s^{-1}$) was nearly twice as much as Gd-DTPA (r_1 = 4.8 $mM^{-1}\,s^{-1}$) and the transversal relaxivity value (r_2 = 35.1 $mM^{-1}\,s^{-1}$) was six times that of Gd-DTPA (r_2 = 5.3 $mM^{-1}\,s^{-1}$). The results showed that the liver and kidneys signal for T_1 and T_2 values improved by at least 26% and up to 70% *in vivo*, which is stronger than Gd-DTPA at the same dose. Majeed et al. [86] also synthesized UMIONs (D = 4.6 ± 0.7 nm) under high magnetization (50 emu g^{-1}) using the water-soluble ligand DDT-PMAA, and modified Dox on the outer layer to achieve the purpose of magnetic targeting therapy; however, this study only discusses cytotoxicity, loading capacity, and magnetism, and does not mention magnetic imaging performance.

There are other methods, for example, Sarlak et al. [87] first synthesized Fe_3O_4 NPs (10 nm) by thermal precipitation method, and then coated hydrophilic cellulose-poly citric acid to obtain the final product (CNC-PCA/Fe_3O_4). The most interesting thing is that the hydrated particle size after coating does not increase, and it also decreases (13.2 to 12 nm), which proves that there is no precipitation after coating, resulting in the high M_s (52.2 emu g^{-1}), so as to produce high r_1 (13.8 $mM^{-1}\,s^{-1}$), r_2 (96.2 $mM^{-1}\,s^{-1}$), and a considerable r_2/r_1 (7.0) at 3.0 T.

Although thermal decomposition can achieve small-scale production (typically 5 g), it does not meet the huge clinical demand; therefore, achieving large-scale and stable production of USIONs has become one of the key preconditions for its clinical application [88], whereas other methods cannot achieve large-scale production because of the constraints of particle size stability and shape constancy [89]. Starsich et al. [90] used flame aerosol technology to prepare different quantities of silica coatings with different proportions of iron(III)acetylacetonate and hexamethyldisiloxane, and focused on structure–function relationships and cytocompatibility. This mode of production of USIONs can achieve stable, uniform, and constant production. The advantage of those prepared USIONs is that iron oxide exists in the form of monomer and its particle size is about 1.5 nm. It has good imaging effect as T_1 contract agent, however, because of silica coating causes a poor T_2 signal, the lethality of the four kinds of cells in the study of configuration and biocompatibility is not more than 15% even when the iron content reaches 1 mg/mL, which proves its potential for application in T_1 signal analysis.

Although the particles coated with ferroferric oxide alone can achieve dual-modulus imaging, their sensitivity cannot meet clinical requirements [91]; therefore, the development of highly sensitive CAs to meet the clinical needs has become one of the burning issues to be solved.

3.2 Application of Fe_3O_4 cladding metal in the outer layer of nanoparticles

Generally, neither Gd-based coordination complexes on the market today nor iron oxide or manganese metals can satisfy the high accuracy of diagnosis in tumor treatment [92]. The main reason is that other highly magnetic metals in the outer layer of nanoparticles can improve the sensitivity of nanoparticles, which can meet the requirements of high-precision imaging in clinical application [93].

Yang et al. [94] relied on this theory to prepare the late-model nanoparticles with cladding metal in the outer layer. The preparation process was as follows: first, polyethylenimine (PEI) coated on the synthesized of Fe_3O_4 NPs surface, then $Gd(acac)_3$ forms the outermost layer at a suitable distance in the outer layer of Fe_3O_4@Gd_2O_3 NPs (YFGN) with an interstitial-hollow space forming a yolk-like structure, which ensures the formation of an ideal T_2 signal due to water molecules can pass through the porous shell and approach Fe_3O_4 nanoparticles in the core [95]. Besides, the special yolk-like structure owned a large specific surface area and mesopore, so that it can be used as a drug delivery system [96], so cisplatin was adsorbed to PEI by the special yolk-like structure. In addition, tumor cells in a slightly environment can produce more protons to replace platinum chelates, so as to achieve the effect of pH response, so cisplatin was released from YFGN through the special yolk-like structure. Final aminating PEG-COOH and folic acid improve the hydrophilicity and achieve the purpose of targeting, thus achieving the goal of complex (FA-PYFGN-CDDP). At 15 min post-injection, responding signal-to-noise ratio (ΔSNR) was 88.53% and 41.71% for T_1 and T_2, respectively, which testified quality targeting and imaging performance for FA-PYFGN. Concurrently, the r_1 and r_2 values of PYFGN were 7.91 and 386.5 $mM^{-1} s^{-1}$, respectively (r_1 value of Gd^{2+} was 4.8 $mM^{-1} s^{-1}$, and the r_2 value of original Fe_3O_4 was 268.1 $mM^{-1} s^{-1}$); however, Gd^{2+} remained in other organs, especially in the kidneys. FA-PYFGN-CDDP showed advanced targeted ability and reduce the side effects of CDDP [97], and the improvement of therapeutic effect was nearly 1.5-fold; however, the retention of gadolinium in kidney and the tedious preparation process limited its practical application.

To effectively reduce the side effects of gadolinium retention, Xiong et al. [98] prepared Fe_3O_4 nanoparticles and coated with MnO_2 to improve diagnostic accuracy and decrease aggregation in the reticuloendothelial system and its toxicity. In the acidic condition of tumors, Mn^{2+} was released and a T_1 signal was produced, which reduced aggregation of nanoparticles in normal tissues; at the same time, the inner Fe_3O_4 produced a T_2 signal, so that the CA with a double signal (in pH response terms) could be achieved. In addition, the stability of Fe_3O_4 coated with carbon is significantly improved, and carbon in the application can make the nanoparticles have other excellent properties in the later research, such as thermotherapy and fluorescence imaging (FL) because carbon possesses various excellent properties of chemically stable, tunable bandgap, good thermal conductivity, and stability [99].

The preparation process is as follows: the carbon shell coated Fe_3O_4 (Fe_3O_4@C, called FOC) nanoparticles were prepared by hydrothermal calcination of ferrocene and hydrogen peroxide at 240°C, and the supernatant was discarded under a magnetic field. Then the oxidative $KMnO_4$ was added; Fe_3O_4@C@MnO_2 (FOCMO, with S_d of 130 nm) nanoparticles were prepared through the oxidation–reduction reaction [100] among the reductive FOC and the oxidative $KMnO_4$. The r_1 was 5.33 $mM^{-1} s^{-1}$, and r_2 = 364.20 $mM^{-1} s^{-1}$ at pH = 5.0 *in vivo* (r_1 = 3.56 $mM^{-1} s^{-1}$, r_2 = 396.57 $mM^{-1} s^{-1}$ at pH = 6.5), which suggested sufficient sensitivity to acidic environment. After intravenous administration of FOCMONPs, T_1 value was enhanced for 127% at 24 h. Furthermore, T_2 value decreased 71% *in vitro*. In addition, the cell viability exhibited even a high (>85%) concentration up to 200 ppm for 24 h with HeLa and $4T_1$ cells, which demonstrated that FOCMO NPs can improve accuracy diagnosis.

3.3 Application of metal-doping-Fe_3O_4 in bimodal imaging

Metal-doping-Fe_3O_4 nanoparticles can be divided into two categories: one is that changing the iron valence to form new nanoparticles, and the other is that doping alone does not change the iron valence.

3.3.1 $M_xFe_{3-x}O_4$

To improve its magnetic sensitivity, Hu and colleagues prepared $Mn_xFe_{3-x}O_4$ by doping manganese into Fe_3O_4 by pyrolysis (MFNPs) [101]. The M_s of the MFNPs gradually increased with increasing Mn^{2+} concentration, and reached 75.5 emu g^{-1} when x = 0.34. The relaxation signal increased with the increase in Mn concentration. When Mn reached 0.34, the maximum values of r_1 and r_2 were

21.5 and 67.2 $mM^{-1} s^{-1}$, respectively. Furthermore, MFNPs showed excellent colloidal stability, including different solutions (H_2O, PBS, and 1 M NaCl solution) and different pH solution (7–11), which showed good prospects for clinical application; however, the article does not cover cytotoxicity effects and *in vivo* imaging.

In the same way, Guldris et al. [102] coated PAA on zinc and manganese doped Fe_3O_4 nanoparticles by a hydrothermal method in gram-scale quantities to prepare ultra-small superparamagnetic iron oxide nanoparticles (USPIOs), and then focused on the changes in their apparent properties, stability, and magnetic properties after different centrifugation time and speeds (namely, one sample (NP-ac) centrifuged at 4,000 rpm for 12 h, and another sample (NP-bc) at 3,000 rpm for 10 min). Interestingly, with the increase in centrifugation time and rotation speed, the hydrated particle size decreased nearly two-fold (35 ± 17 to 18 ± 6 nm), the magnetic saturation strength decreased slightly, whereas the r_2 value increased nearly three-fold, and the r_1 value remained similar, because the nanoparticles coated on the surface were separated with the extension of rotation speed and time, resulting in the decrease in iron content and the increase in the content of the outer layer [103]. Furthermore, NP-ac and mouse stem cells can be co-cultured with rat mesenchymal stem cells for 16 h under physiological conditions without aggregation, whereas NP-bc can only remain for 1 h because of more PAA in the outer layer leading to a five-fold decrease in proteins binding [104], which proved the stability of NP-ac *in vivo*. At the same time, after long-term storage for 10 months, in water and agar media, the signal values of r_1 and r_2 did not decrease, but increased, again indicating NP-ac has excellent stability.

3.3.2 Metal-doping-Fe_3O_4

3.3.2.1 Application of Fe_3O_4 doping other metals in the outer layer

The effective doping of other metals in the outer layer can effectively improve the sensitivity of CA [105]. The dumbbell-hybrid nanotrimers (DB-HNTs) showed dual contrasts such as gold-doping-Fe_3O_4 NPs [106]; however, the preparation process was arduous and complicated. On this basis, Gong et al. [107] covered a manganese ferrite ($MnFe_3O_4$) nanoparticles enhanced dual models effect to overcome the tedious process of preparation, but Mn^{2+} was latent toxicity to human body. Similarly, Zhou et al. [108] showed Gd-embedded-Fe_3O_4 NPs as dual MR contrasts; however, the Gd^{2+} could lead to kidney malfunction [109]. Park et al. [110] also reported uranium-doped Fe_3O_4 nanoparticles (EuIO) as the novel agents. EuIO were synthesized by thermal decomposition method. The outer layer was modified by citric acid (EuIO-Cit). EuIO-Cit produced a higher r_1 value (17.2 $mM^{-1} s^{-1}$, $r_{1Gd\text{-}DTPA}$ = 4.8 $mM^{-1} s^{-1}$) with a smaller r_2/r_1 value (5.2) as well as a high hydrophilicity and smaller size (5 nm), which showed better dual modulus development potential. The same magnetic properties are superior, but there remains the issue of the toxicity of foreign elements.

To solve the side effects caused by doping other metals, Thapa et al. [111] verified nitrodopamine-PEG coated single core truncated cubic Fe_3O_4 NPs (ND-PEG-tNCIOs, the average edge length was 12 nm) to enhance imaging effect. The result showed longitudinal and transverse relaxivity of 32 ± 1.29 $mM^{-1} s^{-1}$ and 791 ± 38.39 $mM^{-1} s^{-1}$ at 1.41 *T* at 30°C, respectively. As nitrodopamine-PEG owned the excellent biocompatibility, it could effectively avoid phagocytosis of the immune system so as to increase the iron content of the target local, thus improving the accuracy of T_2 imaging [112], at the same time, the inner structure of the cube makes it easier to aggregate at the tumors than a spherical structure, which makes the imaging results more accurate [113].

3.3.2.2 Application of Fe_3O_4 doping other metals in the inner core

Although embedding T_1 contrast metal (Gd^{3+}, Eu^{3+}, Ni^{2+}, or Dy^{2+}) into Fe_3O_4 NPs could not only improve the sensitivity of contrast medium, but also provide dual-mode imaging as for the fact that the internal impaction ensured the same magnetic field direction and increases mutually [114], as shown in Figure 5, rare-earth contrast materials occasionally cause nephrogenous systemic fibrosis [77]. Therefore, doping some metals as necessary elements of the body becomes an effective means.

Based on this theory, Lu et al. [115] embedded Mn^{2+} into Fe_3O_4 NPs with hydroxyl-PEG-phosphonic acid through a one-pot reaction (Fe_3O_4/MnO, with a size of 20 nm) to improve synergistically imaging performance with safe and accuracy because Mn^{2+} was T_1-weighted CA [116]. The stability test indicated that the nanoparticles retained a single scattering peak even though their size increased to 35 nm from 21 nm after 21 days in water. The r_2 and r_1 values were 209.6 ± 0.7 and 22.8 ± 0.3 $mM^{-1} s^{-1}$ (*v.* [Fe + Mn]), respectively, which was over five times than commercial Magnevist (4.4 ± 0.3 $mM^{-1} s^{-1}$) in terms of the r_1 value and were higher than pure Fe_3O_4

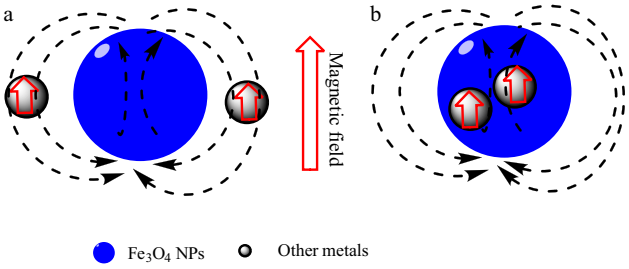

Figure 5: The influence of doping other metals in different positions on magnetic field strength: (a) outer layer; (b) inner layer [115].

NPs and MnO NPs in terms of the r_2 and r_1. Furthermore, the r_2/r_1 ratio was 9.2, which suggested its potential as dual-mode CA [117]. The results of T_1 and T_2 *in vivo* were similar: 5 min after injection, clear images of two kinds of signals could be seen in lung cancer, and 1 h post-injection, the signals could be seen in liver, which indicated that the dual-modulus could be clearly presented and maintained for sufficient time. Despite the excellent imaging results, cytotoxicity and long-term toxicity have not been studied.

4 Janus iron oxides multiple models imaging

Because of the inherent defects of a single CA, such as poor spatial-temporal resolution, low sensitivity, and shallow penetration depth, multi-mode integration of diagnosis and treatment emerged as a need [118]. To this scope, Janus nanomaterials show the potential for multi-mode integration of diagnosis and treatment as its multifaceted modifiability, drug loading ability, and so on, especially for cancer therapy [119]. In this review, Janus multi-models based on MRI imaging, combining one or more of PA, FL, and CT, are described as shown in Figure 6. Of course, there must be other types of multi-model imaging, which will not be discussed in this review.

4.1 FL and MRI

To meet the requirements of noninvasive, real-time, deep-seated tissue responsiveness for cell tracking technology [120], Song et al. [121] prepared Janus Fe_3O_4@PFODBT-COOH (S_d was 51 nm) from poly[2,7-(9,9-dioctylfluorene)-*alt*-4,7-bis(thiophen-2-yl)benzo-2,1,3-thiadiazole](PFODBT, M_w = 10,000–50,000), which exhibited fluorescence property at 680 nm, poly(styrene-*co*-maleic anhydride) (PSMA, M_w = 1,700) which modified the nanoparticle surface with

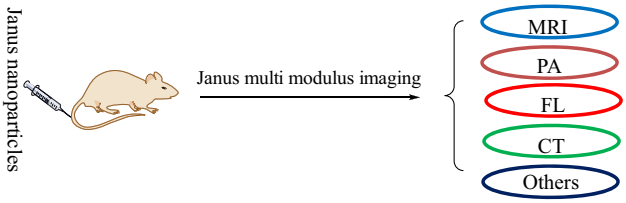

Figure 6: Construction of Janus multi-model imaging.

carboxyl groups to improve stability and prepared Fe_3O_4 nanoparticles by bath sonication. The r_2 signal intensity thereof seven times that commercial Feraheme at the same Fe concentration, at the same Fe concentration, at the same time, the cells were labelled and tracked by the optical properties of semiconductor material PFODPT, which was higher with a signal-to-background ratio of 2.03 at 250 labeled cells, what's more, the FL and MRI signals only decreased by about 20% after 10 days. Although the Janus Fe_3O_4@P-FODBT-COOH used in the present work achieved the combination of optical and magnetic imaging, it cannot meet the development needs of targeted, multi-mode imaging when it was applied only to the applied imaging after cell labeling.

To improve precise diagnostic and effective therapeutic action, Wang et al. [122] reported a simple method to direct assembly of curcumin (anticancer drug), Ce6 (photodynamic agent), and pH-sensitive molecules into polyphosphazene, and coated on Fe_3O_4 NPs to attain the final Janus NPs (FHCPCe NPs, the average size was 100 ± 10 nm). The M_s and r_2 values of the FHCPCe NPs were 64.06 emu g^{-1} and 184.92 mM^{-1} s^{-1}, respectively, which was higher than commercial Fericia. The anti-cancer results showed a hyperintense area for T_2-weighted MRI *in vivo*. More interestingly, over time, the signal at the tumor gradually increased, reaching its maximum value at 8 h, which indicated FHCPCe NPs accumulated at tumor cells because of the targeting properties of polyphosphazene. More importantly, because of Ce6 coupling to the surface of polyphosphatide, easy aggregation of Ce6 in water could be improved, and the fluorescence intensity and the yield of singlet oxygen were significantly increased. Therefore, the FL effect better complements the deficiency of MRI imaging, and a large number of singlet oxygen molecules can kill cancer cells efficiently, thus truly achieving a highly efficient integration of diagnosis and treatment.

4.2 PA and MRI

Janus imaging can facilitate the fast, effective and efficient imaging date, photoacoustic imaging (PA) was

favored by researchers as its compatibility [123]. Bell and colleagues [124] developed a novel Janus model (attachment of Flammas774 to Fe_3O_4, with a size of 150 nm, FeO-774) for both PA and MRI. The reason for using Fe_3O_4-774 is that MRI offers complex anatomic details and PA provides biological- and metabolic-related information [125]. The optoacoustic absorption signal for FeO-774 (with a maximum absorption wavelength of 780 nm) showed the intensity of linear curve between concentration and absorption, which proved that FeO-774 was effective for use in suitable PA probes. The r_2 was 212 $mM^{-1} s^{-1}$ for FeO-774, which was higher than commercial Resovist (r_2 = 151 $mM^{-1} s^{-1}$) [126]. Although the results of *in vivo* imaging indicated that FeO-774 provided not only high-quality PA imaging but also excellent T_2 imaging, the results proved that FeO-774 was not aggregated *in vivo*; however, the author did not consider its toxicity.

To compensate for the deficiency of pure T_2 magnetic imaging, Ren et al. composed core/shell structure Fe_3O_4/Au NPs (of cubic structure with S_d of 51.4 ± 2.8 nm) for dual-modulus imaging of MRI and PA for accurate diagnosis [127]. The magnetic saturation and r_2 values were respectively 97.8 emu g^{-1} and 625.1 $mM^{-1} s^{-1}$. *In vivo* for MRI, the tumor area presented a darker magnetic field of vision after injection, which exhibited higher property for MRI. At the same time, PA imaging showed obvious neovascularization in the tumor area. The combination of the two methods shows a certain potential for clinical application.

4.3 CT and MRI

The combination of positron emission tomography (CT) and MRI is more popular in Janus model because MRI can provide images with excellent soft-tissue details [128], whereas CT imaging can provide a high-3D-resolution information of bone and calcification, so as to repair the defects of MRI, and it has a significant effect on early diagnosis of cancer [129].

To overcome the colloidal instability and poor biocompatibility with an organic layer of oleylamine or oleic acid coated Fe_3O_4 nanoparticles [104], Cui et al. [130] used an inorganic aluminum hydroxide layer to coat on the surface of Fe_3O_4 nanoparticles, and studied the influence of the thickness of aluminum hydroxide on MRI imaging. At the same time, bisphosphonate polyethyleneglycol (BP-PEG) was modified with the help of the phosphate radical on BP-PEG and aluminum to form the covalent coordination of hydroxide on fluoride, which can be used to realize CT and MRI imaging together and improve the accuracy of diagnosis. Interestingly, after filtering, the r_2 signal value of the sample can be increased by at least 1.5 times, which is similar to the results of José Rivas et al. [102]. When the ratio of ferric oxide to aluminum hydroxide is 1:1, the particle size can reach a minimum (21 nm); fluoride can also be effectively adsorbed, which leads to fluoride being located in the liver and spleen rather than being absorbed by bone because of the smaller particle size: this can prolong the blood circulation time [131], so that the sample will not decay in the body for at least 2 h.

To improve the accuracy of diagnosis, Shen and Shi [132] prepared superparamagnetic manganese ferrite (5 nm) using an environment-friendly solvothermal method, and then modified with PEG-dopamine and target material RGD to improve targeting and avoid phagocytosis of RES [133]. With the aid of dopamine and the RGD sulfhydryl group, a ^{64}Cu radiolabel was adsorbed and the final product was obtained, which are targeted nanoparticles with CT and MRI effects (^{64}Cu-NPs-dopa-PEG-DOTA/RGD, S_d = 26.4 ± 7.5 nm). These 5 nm nanoparticles exhibited high M_s (41.7 emu/g) at 15,000 Oe, and the r_2 was then 267.5 $mM^{-1} s^{-1}$ (*v.* [Mn + Fe]), which was more than two times higher than Feridex (*c.*120 $mM^{-1} s^{-1}$) [129]. *In vivo* imaging shows that nanoparticles can effectively gather in tumor areas, and radioactive substances are also more highly concentrated in organs than elsewhere; therefore, CT and MRI imaging effects were significantly improved, which indirectly proves that RGD can indirectly improve CT and MRI effects. In addition, because of the presence of RGD and dopamine, the blood circulation time was significantly increased.

Although MRI/CT dual imaging is realized above, MRI involves single signal imaging, which cannot achieve the accuracy needed for tissue recognition. Zhang et al. [134] wrapped GdF_3 and Fe_3O_4 nanoparticles with PEG to form weighted T_1/T_2 signal and CT imaging capabilities to meet the high demand imposed by cancer diagnosis. In the mixed solution of ethylene glycol and water, PEG, Gd^{3+}, Fe^{3+}, and NH_4F (as a catalyst) were added in turn to form PEG-coated GdF_3:Fe nanoparticles at 100°C (length = 51.9 ± 6.1 nm, width = 31.3 ± 3.5 nm). The M_s of the PEG-GdF_3:Fe NPs (2.38 emu g^{-1} *v.* [Gd + Fe] at 20 kOe) was higher than that of $KGdF_4$ NCs (1.97 emu g^{-1}) [50]. The r_1 and r_2 relaxivity values of the PEG-GdF_3:Fe NPs were 3.3 and 36.0 $mM^{-1} s^{-1}$, respectively, and the r_2/r_1 ratio was 10.2, but PEG-GdF_3:Fe NPs still be used as dual modulus imaging CA, which was analogy with FeCo NPs (r_2/r_1 = 9.2) [135]. The blood circulation time increased because of modified PEG [136], and the nanoparticles

could accumulate effectively at tumor cells. After 1.5 h post-injection, dual-mode imaging could still be obtained clearly. At the same time, CT revealed that the imaging effect was still better than the clinical iobitridol at low dosage. The above results demonstrated the potential of multi-mode Janus imaging.

4.4 CT, FL, and MRI

Recently, the integration of targeted tumor diagnosis and treatment is a method that combines targeted diagnosis and treatment, which has become a powerful method to improve the cure rate. Janus nanoparticles joining three imaging mediums, CT, MRI and FL, can meet the requirements and show the great potential in imaging, diagnosis, and treatment [137].

Marco and colleagues had recently reported a new Janus NPs owning Au NPs with two enzymatic effectors and mesoporous silica coated β-cyclodextrin, which formed pH-responsive supramolecular nanovalve [138]. Dox loaded on porous structure based on the smart nanovalve successfully evaluated the anticancer effect with HeLa cancer cells *in vitro*, showing a significantly improved antitumor effect. However, it cannot achieve the purpose of imaging and real-time tracking simultaneously.

Then they reported again [139] on a novel Janus NPs by combining an Fe_3O_4 NPs/mesoporous silica@Au NPs to form core/shell structure, and modified the targeting peptide (cRGD) and a fluorescent dye. The preparation process is as follows: oleic-capped magnetic ferric oxide nanoparticles (Mag 320) were synthesized according to Liong's method [140], involving cetyltrimethylammonium bromide in a reaction with oleic-capped magnetic ferric oxide nanoparticles in ultrapure water at 60°C under vigorous stirring. After adjusting the pH with sodium hydroxide, TEOS was added, and the magnetic ferric oxide coated with mesoporous SiO_2 (Mag 320@MS) was obtained by electrostatic attraction. Mag 320@MS was emulsified by adding paraffin; after centrifugation and dilution with methanol, Mag 320@MS was reacted with (3-mercaptopropyl)trimethoxysilane, and the product was stirred and compounded with the prepared Au nanoparticles [141] to obtain Janus Au-Magnetic@MS NPs (Janus Au-Mag 320@MS). Catalyzed by NHS and EDAC, Alexa Fluor 647 Hydrazide was modified to Janus Au-Mag 320@MS, then cRGD was modified on the surface in a phosphate buffer by covalently linking, and finally, the fluorescent material was modified on the Janus NPs (RAM, the overall size was 163 ± 2.8 nm). The saturation magnetization value of RAM decreased to 7 emu/g (the M_s of oleic-capped Fe_3O_4 NPs was 33.7 emu/g). Effectively, the low r_2 and r_1 values were 13 and 0.3 $mM^{-1}\,s^{-1}$, respectively, and final r_2/r_1 ratio was 39, which was deemed acceptable against other reported MNPs [142]. This was mainly because of the ideal spatial structure of mesoporous silica, which could make protons pass through smoothly, thus producing resonance signal; however, because of the influence of more coating layer and other metals, the resonance signal was relatively weakened [141]. The fluorescence emission of RAM was not completely quenched, and the intensity of the fluorescence increased with the increase in concentration, which showed excellent optical tracking. The HU experimental values of RAM also increased with the concentration (linear relationship R^2 = 0.9963). No toxicity was found in *HEK293*, *HepG2*, and *RAW 264.7* at 350 μg/mL of RAM *in vitro*. After 2 h of intravenous injection, RAM aggregation could be seen on MRI, which was mainly attributed to the effective targeting of rRGD, and the same results could still be seen on PET-CT (the PET-CT signal was more than twice as strong in terms of HU) and fluorescence tracing (no obvious weakness of fluorescence signal was observed). These results demonstrated the potential of RAM in multi-model imaging for diagnosis.

Whether using single modulus, dual modulus, or Janus-multi-modulus, it is necessary to apply ferric oxide to the accurate diagnosis of diseases. The relevant parts of the article are summarized in Table 1. From Table 1, we conclude that from the T_2 signal to T_1 signal and then to dual modulus mode, the size of nanomaterials is continuously decreasing, and M_s is correspondingly reduced, which relatively reduced the r_2 signal and increased the r_1 signal according to the different imaging methods used. Of course, as the particle size and M_s decrease, this also causes Fe_3O_4 NPs to weaken or even lose some magnetic properties, such as magnetic targeting and magnetic thermotherapy. At present, it is impossible to maintain the excellent magnetic properties on the basis of the dual modulus mode of operation, which needs further research.

5 Other classes

Although the thermo-agents based on Fe_3O_4 NPs have been successfully cured of glioblastoma by intratumoral injection, intravenous injection is the most commonly used method in clinic; however, double ligands or magnetic targeting nanoparticles can effectively transport drugs to tumors after intravenous injection [144]. Grifantini et al.

Table 1: Fe_3O_4 NPs-related data of application in MRI

Name abbreviation	Size/nm	H_d/nm	M_s (emu/g)	r_2 ($mM^{-1}s^{-1}$)	r_1 ($mM^{-1}s^{-1}$)	r_2/r_1	Strength/T
Feridex [143]	4.8	58.5		127.48	—	—	
HEX SPs [26]	15–20 (length), 30 (thickness)	—	44	1.774	0.093	19.08	4.7
Ab-MFPLL [38]	128	170.1		487.94	1.81	270.0	7
SPIONPs@Dex-WSG [41]	—	60.66	44.65	229.7	3.41	67.36	7
PMIDA@Fe_3O_4 [43]	—	61	64	341	102	3.34	11.7
Dy@Fe_2O_3 [46]	4.15	5.3	35	132.2	—	—	1.5
$Zn_{0.44}Fe_{2.56}O_4$ [48]	—	38.9	88.9	803.5	37.2	21.6	1.5
FDPOMs [61]	120	120	7.4	192.06	—	—	
ZUIONs [68]	3.3	7		2.4	1.1	2.2	1
Fe^{3+}@PPOPA-b-Psar [70]	28.6				5.6		3
P_2 [72]	4.8	9.9		20.7	5.3	3.8	1.41
FeGd-HN@Pt@LF/RGD2 [72]	6.6	14.7	8.6	70.71	56.57	1.25	1.5
AuNFs@MPS [78]	90	101	206.1	200	60.57	3.3	3
UMIONs [79]	3.3	4.6	50	35.1	8.3		4.7
CNC-PCA/Fe_3O_4 [85]	10	13.2	52.2	96.2	13.8	7	3
FA-PYFGN [87]	109	289	20.9	386.5	7.91		3
FOCMO [94]	114	143	26.67	364.2	5.33		3
EuIO-Cit [98]	4.9	78.3	42	89.1	17.2	5.18	1.5
ND-PEG-tNCIOs [11]	12	53	66	791	32	24.72	1.41
Fe_3O_4/MnO [115]	21	35	35.2	209.6 [Fe + Mn]	22.8 [Fe + Mn]	9.17	0.5
Fe_3O_4@PFODBT-COOH [121]	42.3	51		13	0.3	39	3
FHCPCe [122]	100		64.06	184.92			0.5
FeO-774 [124]	8	150		212			7
Fe_3O_4/Au [127]	51.4		97.8	625.1			7
64Cu-NPs-dopa-PEG-DOTA/RGD [132]	10	26.4	41.7	267.5			7
PEG-GdF3:Fe NPs [134]	51.9 (length), 31.3 (width)		2.38	36.0	3.3	10.2	1.5
RAM [139]	60	163	7	13	0.3	39	1.5

[145] reported a loading systems of Fe_3O_4 NPs carrying a monoclonal antibody, which was effective accumulation in tumor under the external magnetic field, thereby the dose was only one in 200 of that of MAb. Similarly, Felfoul et al. [146] studied a magnetic navigation system and demonstrated that magnetic targeting can effectively transport drugs to tumors. Similarly, Chen et al. [147] combined double ligand targeting (c(RGDyK) and DSPE-PEG2000) with magnetic targeting to meet the clinical application needs. The results showed that the nanoparticles effectively overcome the problem that magnetic fluid cannot be injected intravenously; this is because of the fact that the dual targeted ligands can effectively locate the nanoparticles to the tumor site [148].

Metal-organic frameworks (MOFs) were considered to be smart materials in biomedical applications and imaging because MOFs were similar to mesoporous silica, but MOF owned adjustable channel and volume [149]. Nejadshafiee et al. [150] adsorbed Fe_3O_4 nanoparticles and 5-fluorouracil (FU) into MOF materials using porous MOF materials, and coated them with FA modified chitosan in the outermost layer to achieve the characteristics of target and pH-responsive drug release (at pH = 5.5, FU release reached 90%). Although the magnetic saturation value decreased because of folic acid modified chitosan effects, the r_2 value increased by nearly 1.4 times because of the porous structure of MOF and the color effect of FU. *In vivo* imaging results showed that the magnetic imaging effect was strong in the tumor area. At the same time, the concentration of iron decreased significantly at 1 h post-injection, and the reduction reached 52.1%, which proved that it had a good metabolic rate and a certain targeting ability.

Similarly, Cong et al. [151] used MOF materials combined with Fe_3O_4 to achieve real-time monitoring of drug transport, targeted drug delivery, and controlled drug release. Fe_3O_4 nanoparticles and Dox were covered by a carton layer. The controlled release of Dox was achieved

only after laser irradiation. In addition, the outer layer of MOF material was coated with FA to achieve targeted drug delivery. The magnetic saturation and r_2 values were 28.41 emu g^{-1} and 59.77 mM^{-1} s^{-1}, respectively, which had a certain potential for magnetic imaging applications.

Fe_3O_4@MOF material analogues exhibit quality-drug loading, release, and self-monitoring, which offer the capacity to improve tumor therapeutic, but the preparation process is complex and difficult to industrialize.

In short, even single modulus imaging, dual modulus imaging, and Janus multi-model imaging are gradually adapting to the high requirements of clinical CAs. At present, the application of CAs has gradually introduced magnetic hyperthermia and iron death therapy from the previous simple imaging to the integration of diagnosis and treatment. Therefore, in the future, the development of contrast media will gradually develop toward the direction of multi-function, high sensitivity, and high biocompatibility.

6 Conclusion

This review summarizes the current status of iron CAs from initial application to current research, from the initial single-modulus T_1 and T_2 signals to the dual-modulus imaging format, while the dual modulus is divided into ultra-small nanoparticles of pure iron either externally or internally doped or coated with other metals, to the present Janus multimodal form, that is, combined with one or all of FL, PA, and CT, to achieve the current clinical demand imposed on CAs, such as high sensitivity, accurate imaging, and non-toxic requirements. Although single modulus imaging has inherent limitations in imaging, it shows more advantages in application, such as magnetic hyperthermia and magnetic targeting. Ultra-small Fe_3O_4 nanomaterials (< 5nm) can achieve the purpose of dual-mode imaging, which is complementary single modulus imaging limitations, but exposed the lack of sensitivity defects, so the introduction of other metals to make up for this defects. However, a variety of complementary methods are needed as for the complexity of clinical diseases, so Janus multi-model imaging has been gradually developed to meet the clinical needs. Similarly, it also partially describes the biological application of CAs, including single application to imaging and targeted drug delivery. Finally, the combination of CAs in other materials is described by MOF materials. The preparation method and the magnetic changes of the CA after modification were compared to provide theoretical support for the study of CAs in later generations.

Acknowledgments: This research was financially supported by Minjiang Scholarship of Fujian Province (No. Min-Gaojiao[2010]-117), Central-government Guided Fund for Local Economic Development (No. 830170778), R&D Fund for Strategic Emerging Industry of Fujian Province (No. 82918001), International Cooperation Project of Fujian Science and Technology Department (No. 830170771), and Teaching and Researching Fund for Young Staff of Fujian Educational Department (No. JT180040).

Conflict of interest: The authors declare no conflict of interest regarding the publication of this paper.

References

[1] Yang L, Sun C, Lin H, Gong X, Zhou T, Deng WT, et al. Sensitive contrast-enhanced magnetic resonance imaging of orthotopic and metastatic hepatic tumors by ultralow doses of zinc ferrite octapods. Chem Mater. 2019;31:1381–90.

[2] Liu G, Hong RY, Guo L, Li YG, Li HZ. Preparation, characterization and MRI application of carboxymethyl dextran coated magnetic nanoparticles. Appl Surf Sci. 2011;257(15):6711–7.

[3] Wu W, He QG, Jiang CZ. Magnetic iron oxide nanoparticles: synthesis and surface functionalization strategies. Nanoscale Res Lett. 2008;3:397–415.

[4] Chen YL, Li M, Hong YN, Lam JWY, Zheng QC, Zhong B. Dual-modal MRI contrast agent with aggregation-induced emission characteristic for liver specific imaging with long circulation lifetime. ACS Appl Mater Inter. 2014;6:10783–91.

[5] Jun YW, Huh YM, Choi JS, Lee JH, Song HT, Kim SJ, et al. Nanoscale size effect of magnetic nanocrystals and their utilization for cancer diagnosis via magnetic resonance imaging. J Am Chem Soc. 2005;16:5732–3.

[6] Mornet S, Vasseur S, Grasset F, Veverka P, Goglio G, Demourgues A, et al. Magnetic nanoparticle design for medical applications. Prog Solid State Ch. 2006;34:237–47.

[7] Kim BH, Lee N, Kim H, An K, Park YI, Choi Y, et al. Large-scale synthesis of uniform and extremely small-sized iron oxide nanoparticles for high-resolution T1 magnetic resonance imaging contrast agents. J Am Chem Soc. 2011;133:12624–31.

[8] Zheng SW, Huang M, Hong RY, Deng SM, Cheng LF, Gao B, Badami D. RGD-conjugated iron oxide magnetic nanoparticles for MRI contrast enhancement and hyperthermia. J Biomater Appl. 2013;28(7):1051–9.

[9] Gao J, Liang G, Cheung JS, Pan Y. Multifunctional yolk-shell nanoparticles: a potential MRI contrast and anticancer agent. J Am Chem Soc. 2008;130:11828–33.

[10] Terreno E, Castelli DD, Viale A, Aime S. Challenges for molecular magnetic resonance imaging. Chem Rev. 2010;110:3019–42.

[11] Dubravka N, Marta J, Jovana P, Danijela V, Tatjana R, Sanja RŠ, et al. Application of iron nanoparticles in contemporary physiology and cell biology research. Rev Adv Meter Sci. 2018;53:74–8.
[12] Leung KC, Xuan S, Zhu X, Wang D, Chak CP, Lee SF, et al. Gold and iron oxide hybrid nanocomposite materials. Chem Soc Rev. 2012;41:1911–28.
[13] Moraes Silva S, Tavallaie R, Sandiford L, Tilley RD, Gooding JJ. Gold coated magnetic nanoparticles: from preparation to surface modification for analytical and biomedical applications. Chem Commun. 2016;52:7528–40.
[14] Lacroix LM, Delpech F, Nayral C, Lachaize S, Chaudret B. New generation of magnetic and luminescent nanoparticles for in vivo real-time imaging. Interface Focus. 2013;3:20120103.
[15] Ban Q, Bai T, Duan X, Kong J. Noninvasive photothermal cancer therapy nanoplatforms via integrating nanomaterials and functional polymers. Biomater Sci. 2017;5:190–210.
[16] Jadhav V, Chikode P, Nikam G, Sabale S. Polyol synthesis and characterization of ZnO@$CoFe_2O_4$ MNP's to study the photodegradation rate of azo and diphenyl type dye. Mater Today Proc. 2016;3:4121–7.
[17] McNamara K, Tofail SA. Nanosystems: the use of nanoalloys, metallic, bimetallic, and magnetic nanoparticles in biomedical applications. Phys Chem Chem Phys. 2015;17:27981–95.
[18] Salihov SV, Ivanenkov YA, Krechetov SP, Veselov MS, Sviridenkova NV, Savchenko AG, et al. Recent advances in the synthesis of Fe_3O_4@AU core/shell nanoparticles. J Magn Magn Mater. 2015;394:173–8.
[19] Wang XM, Guo SW, Li ZQ, Xiao XY, Gu L, Luo Q, et al. Safe and potent MRI contrast agents by complexing gadolinium with enzyme/reduction dual-sensitive branched polymers. Appl Mater Today. 2019;17:92–103.
[20] Mogul R, Getz Kelly JJ, Cable ML, Hebard AF. Synthesis and magnetic characterization of microstructures prepared from microbial templates of differing morphology. Mater Let. 2006;60:19–22.
[21] Yang L, Sun C, Lin H, Gong X, Zhou T, Deng WT, et al. Sensitive contrast-enhanced magnetic resonance imaging of orthotopic and metastatic hepatic tumors by ultralow doses of zinc ferrite octapods. Chem Mater. 2019;31:1381–90.
[22] Skumiel A, Kaczmarek-Klinowska M, Timko M, Molcan M, Rajnak M. Evaluation of power heat losses in multidomain iron particles under the influence of AC magnetic field in RF range. Inter J Ther. 2013;34:655–66.
[23] Xie J, Yan C, Zhang Y, Gu N. Shape evolution of "multi-branched" Mn-Zn ferrite nanostructures with high performance: a transformation of nanocrystals into nanoclusters. Chem Mater. 2013;25:3702–9.
[24] Kikuchi T, Kasuya R, Endo S, Nakamura A, Takai T, Metzler-Nolte N, et al. Preparation of magnetite aqueous dispersion for magnetic fluid hyperthermia. J Magn Magn Mater. 2011;323:1216–22.
[25] Gyergyek S, Makovec D, Jagodič M, Drofenik M, Schenk K, Jordan O, et al. Hydrothermal growth of iron oxide NPs with a uniform size distribution for magnetically induced hyperthermia: Structural, colloidal and magnetic properties. J Alloy Compd. 2017;694:261–71.
[26] Kluenker M, Tahir MN, Dören R, Deuker M, Komforth P, Plana-Ruiz S, et al. Iron oxide superparticles with enhanced MRI performance by solution phase epitaxial growth. Chem Mater. 2018;30:4277–88.
[27] Gunawan AA, Chernomordik BD, Plemmons DS, Deng DD, Aydil ES, Mkhoyan KA. Plasmonic interactions through chemical bonds of surface ligands on PbSe nanocrystals. Chem Mater. 2014;26:3328–33.
[28] Sandiford L, Phinikaridou A, Protti A, Meszaros LK, Cui XJ, Yan Y, et al. Bisphosphonate-anchored PEGylation and radiolabeling of superparamagnetic iron oxide: long-circulating nanoparticles for in Vivo multimodal (T1 MRI-SPECT) imaging. ACS Nano. 2013;7:500–12.
[29] Zhang P, Li QF, Wang J, Shi Y, Ling YF. Effect of PVA fiber on durability of cementitious composite containing nano-SiO_2. Nanotechnol Rev. 2019;8:116–27.
[30] Hong RY, Li JH, Qu JM, Chen LL, Li HZ. Preparation and characterization of magnetite/dextran nanocomposite used as a precursor of magnetic fluid. Chem Eng J. 2009;150:572–80.
[31] Mailander V, Landfester K. Interaction of nanoparticles with cells. Biomacromolecules. 2009;10:2379–400.
[32] Liu D, Wu W, Ling J, Wen S, Gu N, Zhang X. Effective PEGylation of iron oxide nanoparticles for high performance in vivo cancer imaging. Adv Funct Mater. 2011;21:1498–504.
[33] Xie J, Xu C, Kohler N, Hou Y, Sun S. Controlled PEGylation of monodisperse Fe_3O_4 nanoparticles for reduced non-specific uptake by macrophage cells. Adv Mater. 2007;19:3163–6.
[34] Amstad E, Gillich T, Bilecka I, Textor M, Reimhult E. Ultrastable iron oxide nanoparticle colloidal suspensions using dispersants with catechol-derived anchor groups. J Am Chem Soc. 2009;9:4042–8.
[35] Ye M, Qian Y, Tang J, Hu H, Sui M, Shen Y. Targeted biodegradable dendritic MRI contrast agent for enhanced tumor imaging. J Control Rel. 2013;69:239–45.
[36] Liu L, Ye Q, Wu Y, Hsieh WY, Chen CL, Shen HH, et al. Tracking T-cells in vivo with a new nano-sized MRI contrast agent. Nanomedicine. 2012;8:1345–54.
[37] Zatovicova MM, Jelenska L, Hulikova A, Ditte P, Ditte Z, Csaderova L, et al. Monoclonal antibody G250 targeting CA IX: binding specificity, internalization and therapeutic effects in a non-renal cancer model. Int J Oncol. 2014;45:2455–67.
[38] Kubovcikova M, Koneracka M, Strbak O, Molcan M, Zavisova V, Antal I, et al. Poly-L-lysine designed magnetic nanoparticles for combined hyperthermia, magnetic resonance imaging and cancer cell detection. J Magn Magn Mater. 2019;475:316–26.
[39] Blanco-Andujar C, Walter A, Cotin G, Bordeianu C, Mertz D, Felder-Flesch D, et al. Design of iron oxide-based nanoparticles for MRI and magnetic hyperthermia. Nanomedicine. 2016;11:1889–910.
[40] Zhang HH, Chen GH, Yu B, Cong HL. Emerging advanced nanomaterials for cancer photothermal therapy. Rev Adv Mater Sci. 2018;53:131–46.
[41] Yin J, Yin G, Pu X, Huang Z, Yao D. Preparation and characterization of peptide modified ultrasmall superparamagnetic iron oxides used as tumor targeting MRI contrast agent. RSC Adv. 2019;9:19397–407.
[42] Louie A. Multimodality imaging probes: design and challenges. Chem Rev. 2020;110:3146–95.
[43] Demin AM, Pershina AG, Minin AS, Mekhaev AV, Ivanov VV, Lezhava SP, et al. PMIDA-modified Fe_3O_4 magnetic

nanoparticles: synthesis and application for Liver MRI. Langmuir. 2018;34:3449–58.
[44] Bhattacharya D, Baksi A, Banerjee I, Ananthakrishnan R, Maiti TK, Pramanik P. Development of phosphonate modified $Fe_{(1-x)}Mn_xFe_2O_4$ mixed ferrite nanoparticles: novel peroxidase mimetics in enzyme linked immunosorbent assay. Talanta. 2011;86:337–48.
[45] Hu Y, Mignani S, Majoral JP, Shen M, Shi X. Construction of iron oxide nanoparticle-based hybrid platforms for tumor imaging and therapy. Chem Soc Rev. 2018;47:1874–900.
[46] Yin J, Xu F, Qu H, Li C, Liu S, Liu L, et al. Dysprosium-doped iron oxide nanoparticles boosting spin-spin relaxation: a computational and experimental study. Phys Chem Chem Phys. 2019;21:11883–91.
[47] Shi X, Li Z, Ge X, Yang C, Fang B, Wei J, et al. Water-soluble noncovalently engineered graphene-neutral red nanocomposite with photocurrent generating capacity. J Nanosci Nanotechnol. 2012;12:1792–8.
[48] Yang L, Wang Z, Ma L, Li A, Xin J, Wei R, et al. The roles of morphology on the relaxation rates of magnetic nanoparticles. ACS Nano. 2018;12:4605–14.
[49] Yang L, Zhou Z, Liu H, Wu C, Zhang H, Huang G, et al. Europium-engineered iron oxide nanocubes with high T1 and T2 contrast abilities for MRI in living subjects. Nanoscale. 2015;7:6843–50.
[50] Ju Q, Tu D, Liu Y, Li R, Zhu H, Chen J, et al. Amine-functionalized lanthanide-doped $KGdF_4$ nanocrystals as potential optical/magnetic multimodal bioprobes. J Am Chem Soc. 2012;134:1323–30.
[51] Lapčík L, Vašina M, Lapčíková B, Hui D, Otyepková E, Richard W, et al. Materials characterization of advanced fillers for composites engineering applications. Nanotechnol Rev. 2019;8:503–12.
[52] Jia FF, Li GL, Yang B, Yu B, Shen YQ, Cong HL. Investigation of rare earth upconversion fluorescent nanoparticles in biomedical field. Nanotechnol Rev. 2019;8:1–17.
[53] Karthi S, Govindan R, Gangadharan A. Luminomagnetic Nd^{3+} doped fluorapatite coated Fe_3O_4 nanostructures for biomedical applications. Je Am Ceram Soc. 2019;33:2558–68.
[54] Thorat ND, Lemine OM, Bohara RA, Omri K, El Mir L, Tofail SA. Superparamagnetic iron oxide nanocargoes for combined cancer thermotherapy and MRI applications. Phys Chem Chem Phys. 2016;18:21331–9.
[55] Shelat R, Bhatt LK, Khanna A, Chandra S. A comprehensive toxicity evaluation of novel amino acid-modified magnetic ferrofluids for magnetic resonance imaging. Amino Acids. 2019;51:929–43.
[56] Guo SH, Fu DW, Utupova A, Sun DJ, Zhou M, Jin Z, et al. Applications of polymer-based nanoparticles in vaccine field. Nanotechnol Rev. 2019;8:143–55.
[57] Li F, Nie W, Zhang F, Lu G, Lv C, Lv Y, et al. Engineering magnetosomes for high-performance cancer vaccination. ACS Cent Sci. 2019;5:796–807.
[58] Liu G, Qi M, Hutchinson MR, Yang G, Goldys EM. Recent advances in cytokine detection by immunosensing. Biosens Bioelectron. 2016;79:810–21.
[59] Ma K, Liu GJ, Yan L. AIEgen based poly(L-lactic-co-glycolic acid) magnetic nanoparticles to localize cytokine VEGF for early cancer diagnosis and photothermal therapy. Nanomedicine-UK. 2019;12:1191–201.
[60] Mikhail AS, Allen C. Block copolymer micelles for delivery of cancer therapy: transport at the whole body, tissue and cellular levels. J Control Rel. 2009;138:214–23.
[61] Yang T, Niu D, Chen J, He J, Yang S, Jia X, et al. Biodegradable organosilica magnetic micelles for magnetically targeted MRI and GSH-triggered tumor chemotherapy. Biomater Sci. 2019;7:2951–60.
[62] Wei J, Shuai X, Wang R, He X, Li Y, Ding M, et al. Clickable and imageable multiblock polymer micelles with magnetically guided and PEG-switched targeting and release property for precise tumor theranosis. Biomaterials-UK. 2017;145:138–53.
[63] Ngen EJ, Wang L, Kato Y, Krishnamachary B, Zhu W, Gandhi N, et al. Imaging transplanted stem cells in real time using an MRI dual-contrast method. Sci Rep. 2015;5:13628.
[64] Lee DE, Koo H, Sun IC, Ryu JH, Kim K, Kwon IC. Multifunctional nanoparticles for multimodal imaging and theragnosis. Chem Soc Rev. 2012;41:2656–72.
[65] Ja-Young P. Highly water-dispersible PEG surface modified ultra small superparamagnetic iron oxide nanoparticles useful for target-specific biomedical applications. Nanotechnology. 2008;36:365603.
[66] Mishra SK, Kumar SBH, Khushu S, Tripathi RP, Gangenahalli G. Increased transverse relaxivity in ultrasmall superparamagnetic iron oxide nanoparticles used as MRI contrast agent for biomedical imaging. Contrast Media Mole I. 2016;350–61.
[67] Wei H, Bruns OT, Kaul MG, Hansen EC, Barch M, Wisniowska A, et al. Exceedingly small iron oxide nanoparticles as positive MRI contrast agents. Proc Natl Acad Sci USA. 2017;114:2325–30.
[68] Liang G, Han J, Hao Q. Gram-scale preparation of iron oxide nanoparticles with renal clearance properties for enhanced T1-weighted magnetic resonance imaging. ACS Appl Bio Mater. 2018;1:1389–97.
[69] Li Y, Huang Y, Wang Z, Carniato F, Xie Y, Patterson JP, et al. Polycatechol nanoparticle MRI contrast agents. Small. 2016;12:668–77.
[70] Miao Y, Xie F, Cen J, Zhou F, Tao X, Luo J, et al. Fe^{3+} @polyDOPA-b-polysarcosine, a T1-weighted MRI contrast agent via controlled NTA polymerization. ACS Macro Lett. 2018;7:693–98.
[71] Chan N, Laprise-Pelletier M, Chevallier P, Bianchi A, Fortin MA, Oh JK. Multidentate block-copolymer-stabilized ultrasmall superparamagnetic iron oxide nanoparticles with enhanced colloidal stability for magnetic resonance imaging. Biomacromolecules. 2014;15:2146–56.
[72] Xiao W, Legros P, Chevallier P, Lagueux J, Oh JK, Fortin M-A. Superparamagnetic iron oxide nanoparticles stabilized with multidentate block copolymers for optimal vascular contrast inT1-weighted magnetic resonance imaging. ACS Appl Nano Mater. 2018;1:894–907.
[73] Khanafer M, Izquierdo-Lorenzo I, Akil S, Louarn G, Toufaily J, Hamieh T, et al. Silver nanoparticle rings of controllable size: multi-wavelength SERS response and high enhancement of three pyridine derivatives. Chemistry Select. 2016;1:1201–6.
[74] Simon GH, Vopelius-Feldt JV, Fu YJ, Schlegel J, Pinotek G, Wendland MF, et al. Ultrasmall supraparamagnetic iron oxide-enhanced magnetic resonance imaging of antigen-induced arthritis. a comparative study between SHU 555 C,

Ferumoxtran-10, and Ferumoxytol. Invest Radiol. 2006;41:45–52.
[75] Shen Z, Song J, Yung BC, Zhou Z, Wu A, Chen X. Emerging strategies of cancer therapy based on Ferroptosis. Adv Mater. 2018;30:e1704007.
[76] Dixon SJ, Lemberg KM, Lamprecht MR, Skouta R, Zaitsev EM, Gleason CE, et al. Ferroptosis: an iron-dependent form of nonapoptotic cell death. Cell. 2012;149:1060–72.
[77] Krzysztof S, Magdalena C, Magdalena MK, Berta F, Bartłomiej D, Sylwia MW, et al. Toxicity of metallic nanoparticles in the central nervous system. Nanotechnol Rev. 2019;8:175–200.
[78] Shen Z, Liu T, Li Y, Lau J, Yang Z, Fan W, et al. Fenton-reaction-acceleratable magnetic nanoparticles for ferroptosis therapy of orthotopic brain tumors. ACS Nano. 2018;12:11355–65.
[79] Roy E, Patra S, Madhuri R, Sharma PK. Anisotropic gold nanoparticle decorated magnetopolymersome: an advanced nanocarrier for targeted photothermal therapy and dual-mode responsive T_1 MRI imaging. ACS Biomater Sci Eng. 2017;3:2120–35.
[80] Roy E, Patra S, Madhuri R, Sharma PK. Stimuli-responsive poly(N-isopropyl acrylamide)-co-tyrosine@gadolinium: iron oxide nanoparticle-based nanotheranostic for cancer diagnosis and treatment. Colloid Surf B. 2016;142:248–58.
[81] Shin TH, Choi JS, Yun S, Kim IS, Song HT, Kim Y, et al. T_1 and T_2 dual-mode MRI contrast agent for enhancing accuracy by engineered nanomaterials. ACS Nano. 2014;8:3393–401.
[82] Shen Z, Chen T, Ma X, Ren W, Zhou Z, Zhu G, et al. Multifunctional theranostic nanoparticles based on exceedingly small magnetic iron oxide nanoparticles for T1-weighted magnetic resonance imaging and chemotherapy. ACS Nano. 2017;11:10992–1004.
[83] Chen C, Li JG, Luo GQ, Xiong YL, Zhang QS. Size-controlled in situ synthesis and photo-responsive properties of silver/poly (methyl methacrylate) nanocomposite films with high silver content. Appl Sur Sci. 2012;24:10180–4.
[84] Li Z, Tan B, Allix M, Cooper AI, Rosseinsky MJ. Direct coprecipitation route to monodisperse dual-functionalized magnetic iron oxide nanocrystals without size selection. Small. 2008;4:231–9.
[85] Li Z, Yi PW, Sun Q, Lei H, Li H, Zhao HL, et al. Ultrasmall water-soluble and biocompatible magnetic iron oxide nanoparticles as positive and negative dual contrast agents. Adva Funct Mater. 2012;22:2387–93.
[86] Majeed MI, Lu Q, Yan W, Li Z, Hussain I, Tahir MN, et al. Highly water-soluble magnetic iron oxide (Fe_3O_4) nanoparticles for drug delivery: enhanced *in vitro* therapeutic efficacy of doxorubicin and MION conjugates. J Mater Chem B. 2013;1:2874.
[87] Torkashvand N, Sarlak N. Fabrication of a dual T1 and T2 contrast agent for magnetic resonance imaging using cellulose nanocrystals/Fe_3O_4 nanocomposite. Eur Poly J. 2019;118:128–36.
[88] Valencia PM, Farokhzad OC, Karnik R, Langer R. Microfluidic technologies for accelerating the clinical translation of nanoparticles. Nat Nanotechnol. 2012;7:623–9.
[89] Liu CL, Peng YK, Chou SW, Tseng WH, Tseng YJ, Chen HC, et al. One-step, room-temperature synthesis of glutathione-capped iron-oxide nanoparticles and their application in in vivo T1-weighted magnetic resonance imaging. Small. 2014;10:3962–9.
[90] Starsich FHL, Eberhardt C, Keevend K, Boss A, Hirt AM, Herrmann IK, et al. Reduced magnetic coupling in ultrasmall iron oxide T1 MRI contrast agents. ACS Appl Bio Mater. 2018;1:783–91.
[91] Na HB, Song IC, Hyeon T. Inorganic nanoparticles for MRI contrast agents. Adv Mater. 2009;21:2133–48.
[92] Lee YC, Chen DY, Dodd SJ, Bouraoud N, Koretsky AP, Krishnan KM. The use of silica coated MnO nanoparticles to control MRI relaxivity in response to specific physiological changes. Biomaterials-UK. 2012;33:3560–7.
[93] Choi JS, Lee JH, Shin TH, Song H-T, Kim EY, Cheon J. Self-confirming "and" logic nanoparticles for fault-free MRI. J Am Chem Soc. 2010;132:11015–7.
[94] Yang M, Gao L, Liu K, Luo C, Wang Y, Yu L, et al. Characterization of $Fe_3O_4/SiO_2/Gd_2O(CO_3)_2$ core/shell/shell nanoparticles as T1 and T2 dual mode MRI contrast agent. Talanta. 2015;131:661–5.
[95] Kim MH, Son HY, Kim GY, Park K, Huh YM, Haam S. Redoxable heteronanocrystals functioning magnetic relaxation switch for activatable T1 and T2 dual-mode magnetic resonance imaging. Biomaterials-UK. 2016;101:121–30.
[96] Fan W, Shen B, Bu W, Chen F, Zhao K, Zhang S, et al. Rattle-structured multifunctional nanotheranostics for synergetic chemo-/radiotherapy and simultaneous magnetic/luminescent dual-mode imaging. J Am Chem Soc. 2013;135:6494–503.
[97] Sun X, Du R, Zhang L, Zhang G, Zheng X, Qian J, et al. A pH-responsive yolk-like nanoplatform for tumor targeted dual-mode magnetic resonance imaging and chemotherapy. ACS Nano. 2017;11:7049–59.
[98] Xiong LQ, Chen ZG, Yu MX, Li FY, Liu C, Huang CH. Synthesis, characterization, and in vivo targeted imaging of amine-functionalized rare-earth up-converting nanophosphors. Biomaterials-UK. 2009;30:5592–600.
[99] Liu YF, Jiang LY, Wang HN, Wang H, Jiao W, Chen GZ, et al. A brief review for fluorinated carbon: synthesis, properties and applications. Nanotechnol Rev. 2019;8(1):573–86.
[100] Guo W, Qi Y, Zhang Y, Ma L, Yu D, Zhan J. Biocompatible caramelized carbonaceous nanospheres supported paramagnetic ultrathin manganese oxide nanosheets via self-sacrificing reduction as a MRI contrast agent for liver imaging. Carbon. 2016;110:321–9.
[101] Wang L, Wu Q, Tang S, Zeng J, Qiao R, Zhao P, et al. Ultrasmall PEGylated $MnxFe_{3-x}O_4$ (x = 0-0.34) nanoparticles: effects of Mn(ii) doping on T1- and T2-weighted magnetic resonance imaging. RSC Adv. 2013;3:23454.
[102] Guldris N, Argibay B, Kolen'ko YV, Carbo-Argibay E, Sobrino T, Campos F, et al. Influence of the separation procedure on the properties of magnetic nanoparticles: gaining *in vitro* stability and T1-T2 magnetic resonance imaging performance. J Colloid Interf Sci. 2016;472:229–36.
[103] Walkey CD, Olsen JB, Guo H, Emili A, Chan WCW. Nanoparticle size and surface chemistry determine serum protein adsorption and macrophage uptake. J Am Chem Soc. 2012;134:2139–47.
[104] Wang X, Niu D, Wu Q, Bao S, Su T, Liu X, et al. Iron oxide/manganese oxide co-loaded hybrid nanogels as

pH-responsive magnetic resonance contrast agents. Biomaterials-UK. 2015;53:349–57.
[105] Zhou ZJ, Bai RL, Wang ZT, Bryant H, Lang LX, Merkle H, et al. An albumin-binding T1-T2 dual-modal MRI contrast agents for improved sensitivity and accuracy in tumor imaging. Bioconjugate Chem. 2019;30:1821–9.
[106] Cheng K, Yang M, Zhang RP, Qin CX, Su XH, Cheng Z. Hybrid nanotrimers for dual T_1 and T_2-weighted magnetic resonance imaging. ACS Nano. 2014;8:9884–96.
[107] Gong M, Yang H, Zhang S, Yang Y, Zhang D, Li Z, et al. Targeting T1 and T2 dual modality enhanced magnetic resonance imaging of tumor vascular endothelial cells based on peptides-conjugated manganese ferrite nanomicelles. Int J Nanomed. 2016;11:4051–63.
[108] Zhou Z, Huang D, Bao J, Chen Q, Liu G, Chen Z, et al. A synergistically enhanced T(1) -T(2) dual-modal contrast agent. Adv Mater. 2012;24:6223–8.
[109] Kanal E, Tweedle MF. Residual or retained gadolinium: practical implications for radiologists and our patients. Radiology. 2015;275:630–4.
[110] Park JC, Lee GT, Kim HK, Sung B, Lee Y, Kim M, et al. Surface design of Eu-doped iron oxide nanoparticles for tuning the magnetic relaxivity. ACS Appl Mater Interf. 2018;10:25080–9.
[111] Thapa B, Diaz-Diestra D, Santiago-Medina C, Kumar N, Tu K, Beltran-Huarac J, et al. T1- and T2-weighted magnetic resonance dual contrast by single core truncated cubic iron oxide nanoparticles with abrupt cellular internalization and immune evasion. ACS Appl Bio Mater. 2018;1:79–89.
[112] Champion JA, Mitragotri S. Role of target geometry in phagocytosis. Proc Natl Acad Sci USA. 2006;103:4930–4.
[113] Park JH, Von Maltzahn G, Zhang L, Schwartz MP, Ruoslahti E, Bhatia SN, et al. Magnetic iron oxide nanoworms for tumor targeting and imaging. Adv Mater. 2008;20:1630–5.
[114] Ban I, Stergar J, Maver U. NiCu magnetic nanoparticles: review of synthesis methods, surface functionalization approaches, and biomedical applications. Nanotechnol Rev. 2018;7(2):187–207.
[115] Lu C, Dong P, Pi L, Wang Z, Yuan H, Liang H, et al. Hydroxyl-PEG-phosphonic acid-stabilized superparamagnetic manganese oxide-doped iron oxide nanoparticles with synergistic effects for dual-mode MR imaging. Langmuir. 2019;35:9474–82.
[116] Zhao Z, Fan H, Zhou G, Bai H, Liang H, Wang R, et al. Activatable fluorescence/MRI bimodal platform for tumor cell imaging via MnO_2 nanosheet-aptamer nanoprobe. J Am Chem Soc. 2014;136:11220–3.
[117] Caravan P, Ellison JJ, McMurry TJ, Lauffer RB. Gadolinium(III) chelates as MRI contrast agents: structure, dynamics, and applications. Chem Rev. 1999;99:2293–352.
[118] Marciello M, Pellico J, Fernandez-Barahona I, Herranz F, Ruiz-Cabello J, Filice M. Recent advances in the preparation and application of multifunctional iron oxide and liposome-based nanosystems for multimodal diagnosis and therapy. Interface Focus. 2016;6:20160055.
[119] Shao D, Li J, Zheng X, Pan Y, Wang Z, Zhang M, et al. Janus "nano-bullets" for magnetic targeting liver cancer chemotherapy. Biomaterials-UK. 2016;100:118–33.
[120] Ahrens ET, Bulte JW. Tracking immune cells in vivo using magnetic resonance imaging. Nat Rev Immunol. 2013;13:755–63.
[121] Song G, Chen M, Zhang Y, Cui L, Qu H, Zheng X, et al. Janus iron oxides @ semiconducting polymer nanoparticle tracer for cell tracking by magnetic particle imaging. Nano Lett. 2018;18:182–9.
[122] Jing X, Zhi Z, Jin L, Wang F, Wu Y, Wang D, et al. pH/redox dual-stimuli-responsive cross-linked polyphosphazene nanoparticles for multimodal imaging-guided chemo-photodynamic therapy. Nanoscale. 2019;11:9457–67.
[123] Garcia J, Tang T, Louie AY. Nanoparticle-based multimodal PET/MRI probes. Nanomedicine-UK. 2015;10:1343–59.
[124] Bell G, Balasundaram G, Attia ABE, Mandino F, Olivo M, Parkin IP. Functionalised iron oxide nanoparticles for multimodal optoacoustic and magnetic resonance imaging. J Mater Chem B. 2019;7:2212–9.
[125] Peng YK, Lui CN, Lin TH, Chang C, Chou PT, Yung KK, et al. Multifunctional silica-coated iron oxide nanoparticles: a facile four-in-one system for in situ study of neural stem cell harvesting. Faraday Discuss. 2014;175:13–26.
[126] Wang YX. Superparamagnetic iron oxide based MRI contrast agents: current status of clinical application. IEEE Tran Magn. 2011;1:35–40.
[127] Kang N, Xu D, Han Y, Lv X, Chen Z, Zhou T, et al. Magnetic targeting core/shell Fe_3O_4/Au nanoparticles for magnetic resonance/photoacoustic dual-modal imaging. Mater Sci Eng C Mater Biol Appl. 2019;98:545–9.
[128] Ni D, Zhang J, Bu W, Zhang C, Yao Z, Xing H, et al. PEGylated $NaHoF_4$ nanoparticles as contrast agents for both X-ray computed tomography and ultra-high field magnetic resonance imaging. Biomaterials-UK. 2016;76:218–25.
[129] Hwang DW, Ko HY, Lee JH, Kang H, Ryu SH, Song IC, et al. A nucleolin-targeted multimodal nanoparticle imaging probe for tracking cancer cells using an aptamer. J Nucl Med. 2010;51:98–105.
[130] Cui X, Belo S, Kruger D, Yan Y, De Rosales RT, Jauregui-Osoro M, et al. Aluminium hydroxide stabilised $MnFe_2O_4$ and Fe_3O_4 nanoparticles as dual-modality contrasts agent for MRI and PET imaging. Biomaterials-UK. 2014;35:5840–6.
[131] Phillips MA, Gran ML, Peppas NA. Targeted nanodelivery of drugs and diagnostics. Nano Today. 2010;5:143–59.
[132] Shi X, Shen L. Integrin alphavbeta3 receptor targeting PET/MRI dual-modal imaging probe based on the $^{(64)}$Cu labeled manganese ferrite nanoparticles. J Inorg Biochem. 2018;186:257–63.
[133] Yang X, Hong H, Grailer JJ, Rowland IJ, Javadi A, Hurley SA, et al. cRGD-functionalized, dox-conjugated, and $^{(64)}$Cu-labeled superparamagnetic iron oxide nanoparticles for targeted anticancer drug delivery and PET/MR imaging. Biomaterials-UK. 2011;32:4151–60.
[134] Dong L, Zhang P, Lei P, Song S, Xu X, Du K, et al. PEGylated GdF_3:Fe nanoparticles as multimodal T1/T2-weighted MRI and X-ray CT imaging contrast agents. ACS Appl Mater Interf. 2017;9:20426–34.
[135] Seo WS, Lee JH, Sun X, Suzuki Y, Mann D, Liu Z, et al. FeCo/graphitic-shell nanocrystals as advanced magnetic-resonance-imaging and near-infrared agents. Nat Mater. 2006;5:971–6.
[136] Liu Z, Robinson JT, Sun XM, Dai HJ. PEGylated nanographene oxide for delivery of water-insoluble cancer drugs. J Am Chem Soc. 2008;130:10876–7.

[137] Zhang H, Alifu N, Jiang T, Zhu Z, Wang Y, Hua J, et al. Biocompatible aggregation-induced emission nanoparticles with red emission for in vivo three-photon brain vascular imaging. J Mater Chem B. 2017;5:2757–62.
[138] Diez P, Sanchez A, Gamella M, Martinez-Ruiz P, Aznar E, De La Torre C, et al. Toward the design of smart delivery systems controlled by integrated enzyme-based biocomputing ensembles. J Am Chem Soc. 2014;136:9116–23.
[139] Sanchez A, Ovejero Paredes K, Ruiz-Cabello J, Martinez-Ruiz P, Pingarron JM, Villalonga R, et al. Hybrid decorated core@shell Janus nanoparticles as a flexible platform for targeted multimodal molecular bioimaging of cancer. ACS Appl Mater Interf. 2018;10:31032–43.
[140] Liong M, Lu J, Kovochich M, Xia T, Ruehm SG, Nel AE, et al. Multifunctional inorganic nanoparticles for imaging, targeting, and drug delivery. ACS Nano. 2008;2:889–96.
[141] Zemtsova EG, Ponomareva AN, Arbenin AY, Smirnov VM. Structural organization of the magnetic part of smart material in pores of MCM-41 mesoporous silica for target drug delivery. Rev Adv Mater Sci. 2018;57:175–82.
[142] Zahraei M, Marciello M, Lazaro-Carrillo A, Villanueva A, Herranz F, Talelli M, et al. Versatile theranostics agents designed by coating ferrite nanoparticles with biocompatible polymers. Nanotechnology. 2016;25:255702.
[143] Uang J, Bu LH, Xie J, Chen K, Cheng Z, Li XG, et al. Effects of nanoparticle size on cellular uptake and liver MRI with polyvinylpyrrolidone-coated iron oxide nanoparticles. ACS Nano. 2010;4:7151–60.
[144] Han W, Yin G, Pu X, Chen X, Liao X, Huang Z. Glioma targeted delivery strategy of doxorubicin-loaded liposomes by dual-ligand modification. J Biomat Sci-Polyme. 2017;28:1695–712.
[145] Grifantini R, Taranta M, Gherardini L, Naldi I, Parri M, Grandi A, et al. Magnetically driven drug delivery systems improving targeted immunotherapy for colon-rectal cancer. J Control Rel. 2018;280:76–86.
[146] Felfoul O, Mohammadi M, Taherkhani S, De Lanauze D, Zhong Y, Xu D, et al. Magneto-aerotactic bacteria deliver drug-containing nanoliposomes to tumour hypoxic regions. Nat Nanotechnol. 2016;11:941–7.
[147] Chen L, Wu Y, Wu H, Li J, Xie J, Zang F, et al. Magnetic targeting combined with active targeting of dual-ligand iron oxide nanoprobes to promote the penetration depth in tumors for effective magnetic resonance imaging and hyperthermia. Acta Biomater. 2019;96:491–504.
[148] Zheng SW, Liu G, Hong RY, Li HZ, Li YG, Wei DG. Preparation and characterization of magnetic gene vectors for targeting gene. Appl Surf Sci. 2012;259:201–7.
[149] Rojas S, Devic T, Horcajada P. Metal organic frameworks based on bioactive components. J Mater Chem B. 2017;5:2560–73.
[150] Nejadshafiee V, Naeimi H, Goliaei B, Bigdeli B, Sadighi A, Dehghani S, et al. Magnetic bio-metal-organic framework nanocomposites decorated with folic acid conjugated chitosan as a promising biocompatible targeted theranostic system for cancer treatment. Mater Sci Eng C Mater Biol Appl. 2019;99:805–15.
[151] Xu Y, Shan Y, Zhang Y, Yu B, Shen Y, Cong H. Multifunctional Fe_3O_4@C-based nanoparticles coupling optical/MRI imaging and pH/photothermal controllable drug release as efficient anti-cancer drug delivery platforms. Nanotechnology. 2019;30:425102.